Journal of Earth Science, *Vol. 32*, *No. 5*, *p. 1139–1151*, *October 2021* *ISSN 1674-487X*
Printed in China
https://doi.org/10.1007/s12583-021-1425-z

Co-Seismic Surface Rupture and Recurrence Interval of Large Earthquakes along Damaoyaba-Litang Segment of the Litang Fault on the Eastern Margin of the Tibetan Plateau in China

Shiyuan Wang[1], **Rongjun Zhou**[*1], **Mingjian Liang**[1], **Shao Liu**[1], **Nina Liu**[2], **Jianyu Long**[1]
1. *Sichuan Earthquake Agency*, *Chengdu* 610041, *China*
2. *School of Geological Engineering and Geomatics*, *Chang'an University*, *Xi'an* 710054, *China*
Shiyuan Wang: https://orcid.org/0000-0002-8735-2193; Rongjun Zhou: https://orcid.org/0000-0003-4481-6901

ABSTRACT: The Litang fault is a left-lateral secondary shear zone in the Sichuan-Yunnan active block that accommodates the tectonic deformation associated with the eastward extrusion of the upper crust of the Tibetan Plateau. Based on 1 : 50 000 geological mapping of active faults, the Litang fault consists of three geometric segments, the Cuopuhu, Damaoyaba, and Litang segments, in the west of Litang, which are divided by the of Haizi Mountain uplift and the wide-angle bending and branching of the fault near Jinchanggou. This study also identifies the surface rupture of the A.D. 1890 earthquake, which is distributed intermittently along the ~28 km long Damaoyaba segments and ~25 km long Litang segments. The maximum horizontal displacement is 4.1 m along Damaoyaba segments, and 4 m along Litang segments. The rupture involves typical left-lateral shear movement. The two ruptures are divided by discontinuous segments or gaps that are ~18 km long; thus, the total surface rupture is approximately 71 km long. The estimated moment magnitude was M_w7.3±0.1. A comprehensive analysis of data obtained from 5 trenches excavated along the Damaoyaba and Litang segments and the trench data by Xu et al. (2005) identifies age constraints of the 4 most recent paleoseimic events occurred B.C. 1468±54–1340±25, B.C. 52±25–A.D. 76±47, A.D. 1115±90, and A.D. 1890, respectively. The recurrence intervals are 1 415±80, 1 104±104, and 775±90 a, which are consistent with quasi-periodic earthquake recurrence behavior. The average recurrence interval is 1 098±112 a.

KEY WORDS: Litang fault, surface rupture, active fault, recurrence intervals, paleoearthquake, eastern Tibetan Plateau.

0 INTRODUCTION

The eastward extrusion of the Tibetan Plateau has resulted in the formation and southeastward escaping of the Sichuan-Yunnan active block (Fig. 1).

The tectonic deformation is caused by the convergence of the Indian and Eurasian plates (Tapponnier et al., 2001; Molnar and Tapponnier, 1975). The Litang fault is a left-lateral secondary shear zone in the Sichuan-Yunnan Block (Zhang et al., 2013; Xu et al., 2003) that consists of multiple secondary faults arranged in an en-echelon pattren. It extends northwestward from Cuopuhu, through southeast across the Damaoyaba Basin, Litang, Jiawa, and Dewu, and ends near Shawan in Muli County with a total length of ~385 km (striking ~N135°E) (Zhou et al., 2007, 2005). Previous studies of the latest surface activity of the Litang fault have mostly focused on the geometric characteristics, spatial distribution of the fault and the most recent co-seismic surface rupture (Chevalier et al., 2016; Xu et al., 2005; Zhou et al., 2005; Tang and Han, 1993) and have obtained a left-lateral slip-rate of 2–4 mm/yr since the Late Quaternary. However, the age of the co-seismic surface rupture is still under debate. Large earthquakes along the fault and adjacent faults had offered crucial quantitative restriction to the understanding of earthquake recurrences (Yan et al., 2018). Few studies have examined the recurrence behavior of large earthquakes along Litang fault.

From 2012 to 2014, we conducted 1 : 50 000 geological mapping of the Litang fault in the west of Litang. During the nearly 3-year work on the fault, we calculated an average horizontal slip rate of the fault and dug 7 new trenches and combining the results with the findings of previous studies (He et al., 2018). We also developed a new understanding of the geometric characteristics of the latest surface activity of the fault, the spatial distribution and date of the most recent large earthquake, and the recurrence behavior of large earthquakes on the fault.

1 GEOMETRIC STRUCTURE AND CO-SEISMIC SURFACE RUPTURE

Based on the interpretation of advanced land observing satellite (ALOS) satellite images (resolution 2.5 m) and aerial photographs, geological mapping of active faults, we indicate

*Corresponding author: 544756125@qq.com

Manuscript received November 4, 2020.
Manuscript accepted January 29, 2021.

Wang, S. Y., Zhou, R. J., Liang, M. J., et al., 2021. Co-Seismic Surface Rupture and Recurrence Interval of Large Earthquakes along Damaoyaba-Litang Segment of the Litang Fault on the Eastern Margin of the Tibetan Plateau in China. *Journal of Earth Science*, 32(5): 1139–1151. https://doi.org/10.1007/s12583-021-1425-z. http://en.earth-science.net

that the most recent surface activity along Litang fault can be divided into three segments: the Cuopuhu segment, Damaoyaba segment, and Litang segment, between Dong'ou and Gari Mountain. These segments are separated by the ~10-kilometer-wide Haizi Mountain uplift and the wide-angle bending and branching of the fault near Jinchanggou (Figs. 1 and 2).

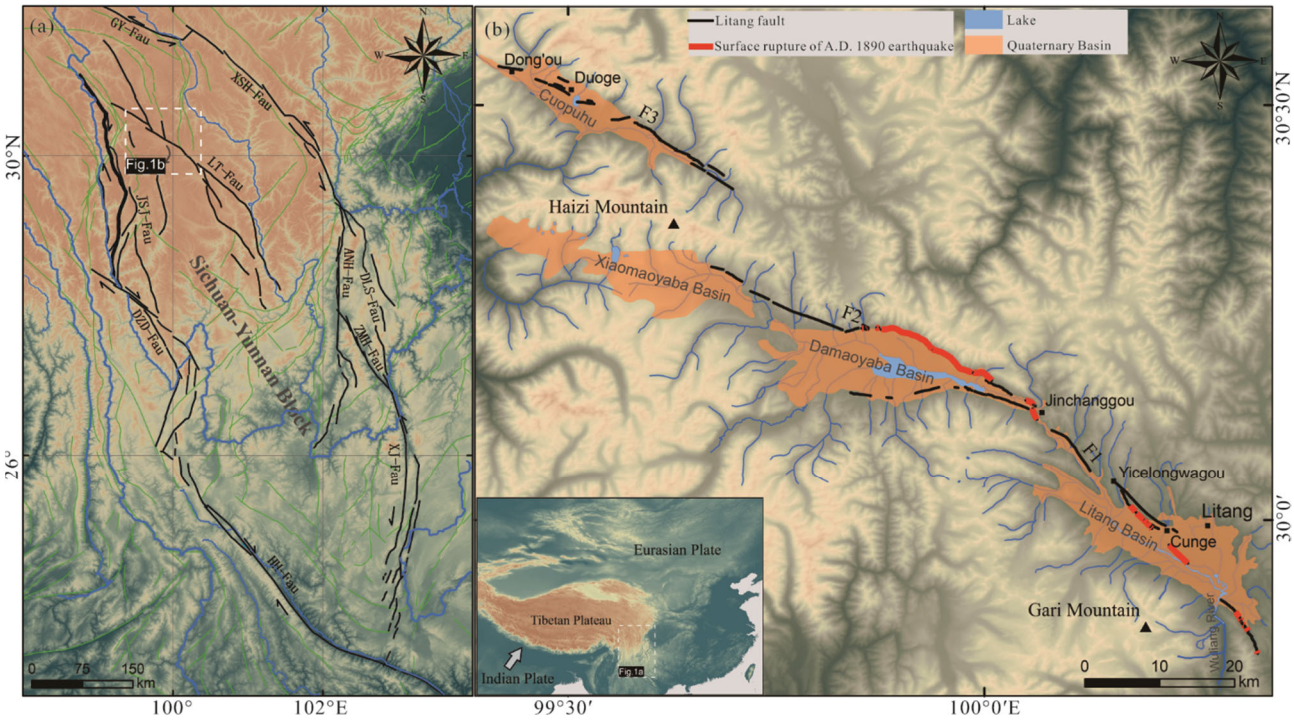

Figure 1. Index maps of the study area. (a) Black lines indicate the major strike-slip faults in the Sichuan-Yunnan Block. LT-Fau. Litang fault; GY-Fau. Garze-Yushu fault; XSH-Fau. Xianshuihe fault; ANH-Fau. Anninghe fault; ZMH-Fau. Zemuhe fault; DLS-Fau. Daliangshan fault; XJ-Fau. Xiaojiang fault; JSJ-Fau. Jinshajiang fault; DZD-Fau. Deqin-Zhongdiang-Daju fault; HH-Fau. Honghe fault. (b) Geometric structure of the Litang fault. F1. Litang segment; F2. Damaoyaba segment; F3. Cuopuhu segment. Thick red lines show the surface ruptures of A.D. 1980 earthquake. The large arrow indicates the motion of the Indian Plate relative to the Eurasian Plate.

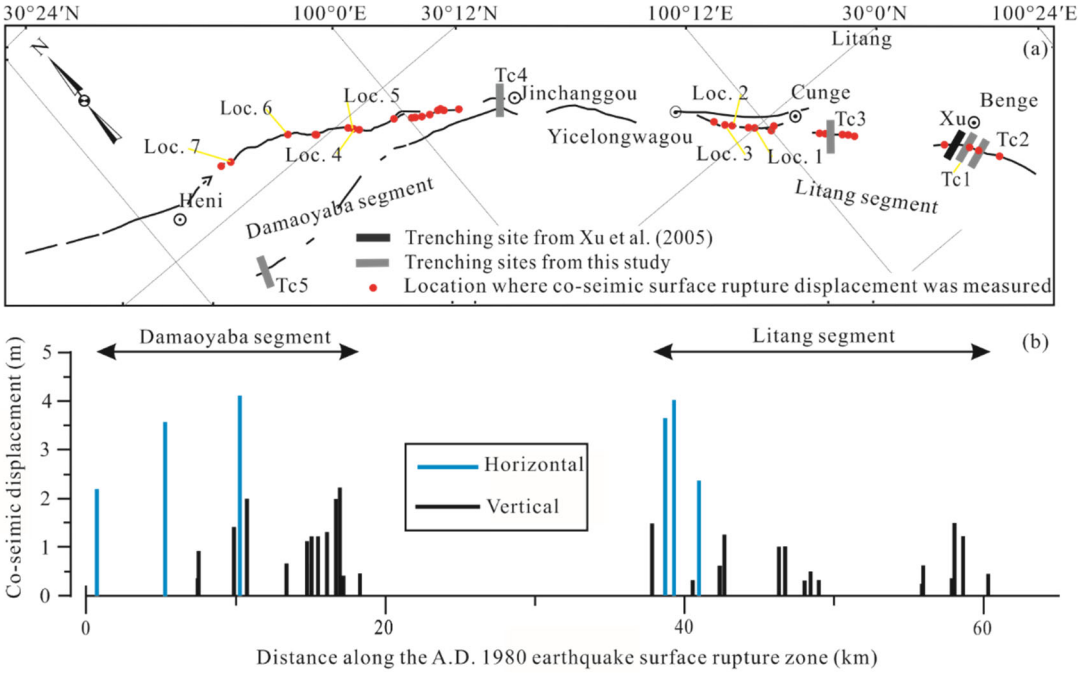

Figure 2. Slip distribution of co-seismic displacements measured along the A.D. 1980 earthquake surface rupture zone along the Damaoyaba segment and Litang segment of Litang fault. (a) Red points show locations where co-seimic surface rupture displacement was measured. Small colored rectangles show trenching sites from this study (gray), Xu et al. (2005) (black); (b) Measured co-seismic displacements of the A.D. 1980 earthquake. Each slip amount was measured at an individual co-seismic surface rupture.

(1) Cuopuhu segment. The fault is generally located along the piedmont on the northern rim of the Cuopuhu Basin. The fault left-laterally offsets gullies, alluvial fans, ridges, and moraine crests and has formed faulted landforms, including fault valleys, fault scarps, and shutter ridges (Figs. 3a–3d). The fault strikes NW to NWW and is nearly EW in some locations. Near

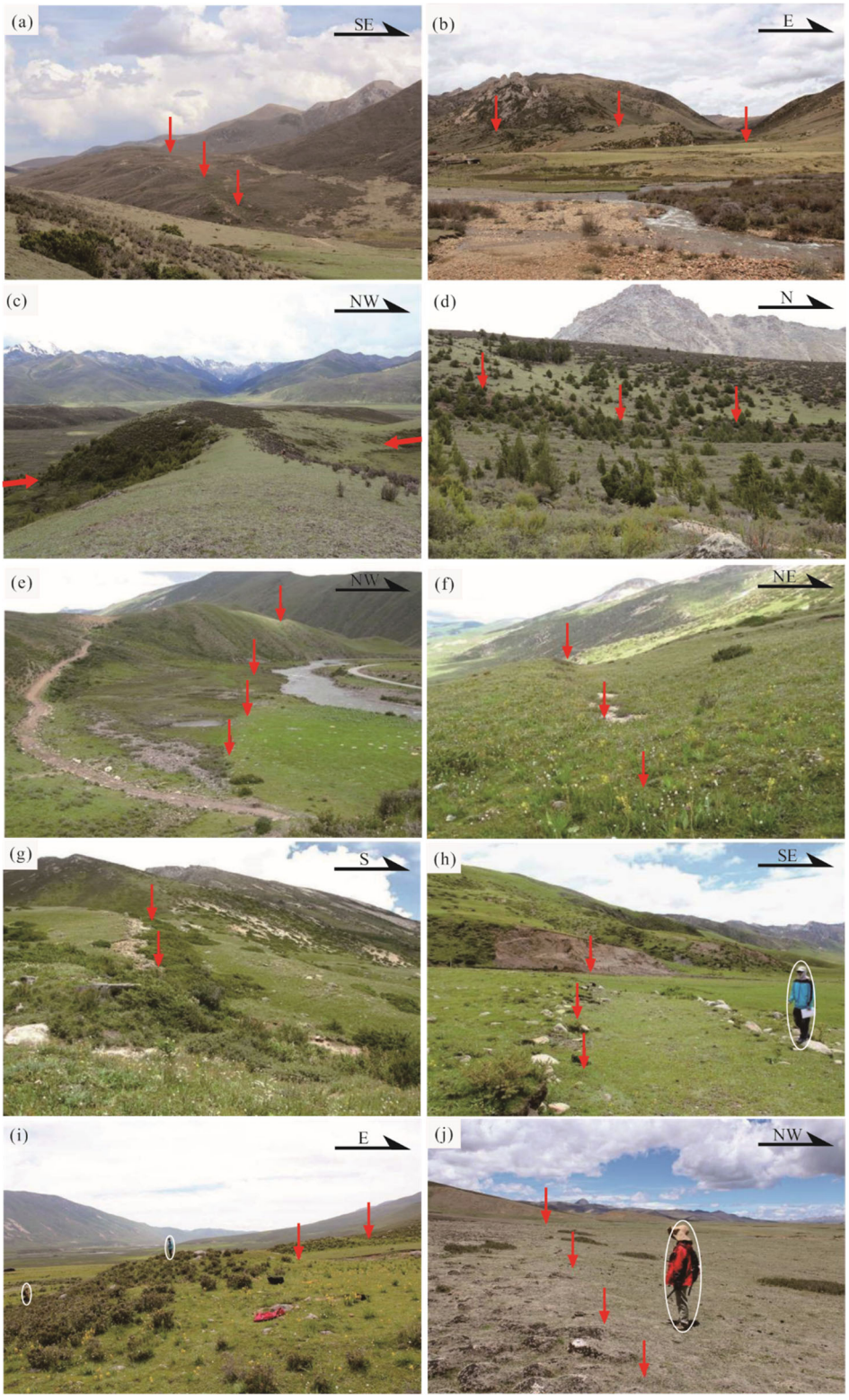

Figure 3. Photographs of representative tectonic landforms of the Cuopuhu segment, including (a) a little linear valley marked by red arrows through the piedmont; (b) a shutter ridge; (c) the offset moraine crests; (d) normal fault scarps. Photographs of representative tectonic landforms and co-seismic surface rupture zones of the Damaoyaba segment, including: (e) fault scarps (approximately 0.2–0.4 m high) on the I-level terrace of the Wuliang River; (f) fault scarps formed by the fault cutting through the piedmont alluvial fan; (g) nearly east-west co-seismic surface rupture zone; (h) surface rupture zone on the I-level river terrace; (i) reverse fault scarps on an alluvial fan; (j) fault scarps (approximately 0.5–1.0 m high). Person circled for scale in (h), (i) and (j).

Duoge-Dong'ou at the northwestern end of the fault, the fault forms 2–3 branches of nearly parallel normal faults, which form a pull-apart at the end of the strike-slip fault. (2) Damaoyaba segment. The fault splits into two branches (southern and northern), which converge near Jinchanggou to the southeast. The main fault is located along the northern edge of the Damaoyaba basin, while its northwestern end cuts into the Xiaomaoyaba Basin and disappears with reverse strike-slip movement (Xu et al., 2005) along distributed co-seismic surface rupture zones (Figs. 3e–3g). The southern secondary fault is generally located along the southern rim of the Damaoyaba Basin, where it has normal strike-slip movement (Figs. 3h–3j). (3) Litang segment. The fault begins at Jinchanggou in the northwest and extends into the rocky mountain area to the southeast. It splits into two branches after reaching Yicelongwagou. The main fault extends along the northern rim of the Litang Basin to Cunge Village and then extends into the basin. Outcrops of the main fault in the basin are discontinuous because it is significantly covered by modern riverbeds, floodplains, and recent alluvial fans; co-seismic surface ruptures are only expressed on the I-level river terrace surface, and the main fault has nearly pure shear movement. The fault is located in front of Gari Mountain after extending beyond the Litang Basin and connects to the Litang-Dewu fault in the watershed of Litang (Figs. 4a–4e).

These observations indicate that the traces of the latest surface activity of the Litang fault are complex; they mainly appear in the form of intermittent extensional features, en-echelon, branches, parallel traces, and changes in strike. The most remarkable feature is the surface rupture zone on the Litang Basin and the northern edge of Damaoyaba Basin. The surface rupture zone in the Litang Basin begins at the watershed to the south of Litang. It extends through the piedmont area of Gari Mountain and into the Litang Basin, where it has an intermittent distribution, extends to the piedmont alluvial fan at Cunge Village and disappears at Yicelongwagou with a total length of ~25 km. The rupture zone forms sag ponds and relatively continuous reverse fault scarps on the piedmont alluvial fans of Gari Mountain. The reverse scarps are ~0.2–1.5 m high and mostly appear as torn turf and tiles at the surface. On the I-level terrace of the Wuliang River, the rupture zone forms a reverse fault scarp ~0.5–2.0 m high. Some segments show evidence of erosion by water that occurred at a later stage. The surface mostly contains microlandforms of turf tears and tiles, NEE-oriented fractures, and nearly NS saddle-like pressure ridges. On the piedmont alluvial fan near Cunge Village, the rupture zone left-laterally offsets a series of gullies. The co-seismic horizontal displacement is ~2.4–4 m. A series of reverse scarps with heights of ~0.3–1.5 m are also present (Figs. 2a, 2b and Table 1).

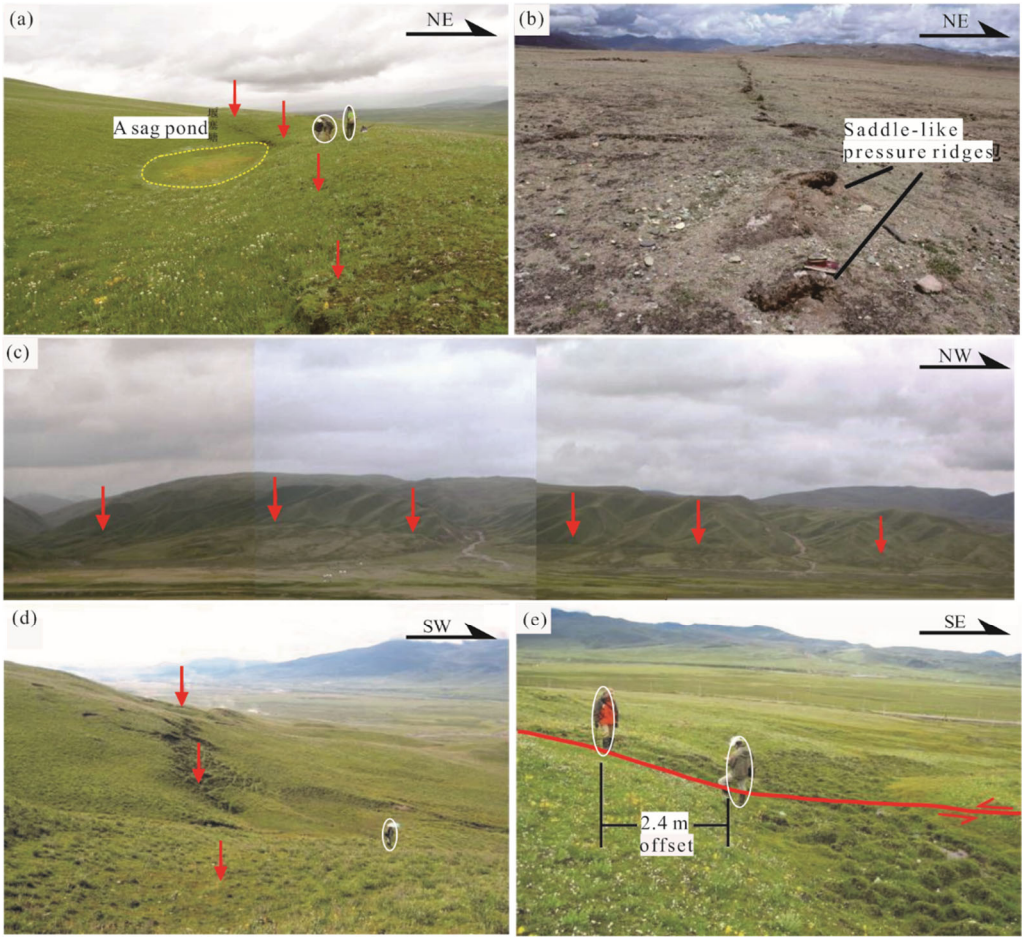

Figure 4. Photographs of representative tectonic landforms and co-seismic surface rupture zones of the Litang segment. (a) Reverse fault scarps and a sag pond on an alluvial fan; (b) saddle-like pressure ridges; (c) fault trace by red arrows at the southern end of the Litang Basin; (d) surface rupture zone; (e) co-seismic left-lateral offset of a gully (approximately 2.4 m) (Fig. 2, Loc. 1). Person circled for scale in (a), (d) and (e).

Table 1 Locations of measurements of co-seismic displacements of the A.D. 1980 earthquake

No.	Longitude (°E)	Latitude (°N)	*H* (m)	*V* (m)	Marker	Figure
a. Litang Basin (Litang segment)						
1	100.305 03	29.886 05		1.5	Alluvial fan	
2	100.304 33	29.886 97		0.2–0.5	Alluvial fan	
3	100.291 19	29.900 17		0.6	Alluvial fan	
4	100.290 67	29.900 67		0.2–0.4	Alluvial fan	
5	100.307 75	29.881 19		1.2	Alluvial fan	
6	100.316 97	29.868 03		0.3–0.6	Alluvial fan	
7	100.244 52	29.948 55		0.3	Terrace	
8	100.240 52	29.952 13		0.5	Terrace	
9	100.237 76	29.954 67		0.3	Terrace	
10	100.228 63	29.963 35		1	Terrace	
11	100.225 77	29.966 50		1	Terrace	
12	100.203 25	29.992 39		1–1.5	Alluvial fan	
13	100.191 38	30.000 61	2.4		Gully	Loc. 1, Fig. 4e
14	100.188 05	30.003 33		0.3	Alluvial fan	
15	100.179 69	30.012 19	4		Gully	Loc. 2
16	100.175 78	30.016 14	3.6		Gully	Loc. 3
17	100.171 08	30.022 64		1.5	Alluvial fan	
18	100.199 88	29.991 35		0.6	Alluvial fan	
b. Damaoyaba Basin, Northern Edge (Damaoyaba segment)						
19	100.001 91	30.168 69		1.1	Alluvial fan	
20	100.004 22	30.167 39		1.2	Alluvial fan	
21	100.008 41	30.165 39		1.2	Alluvial fan	
22	100.013 31	30.162 61		1.3	Alluvial fan	
23	100.019 36	30.160 75		2	Alluvial fan	
24	100.021 50	30.159 61		2.2	Alluvial fan	
25	100.022 86	30.157 83		0.4	Alluvial fan	
26	100.032 42	30.151 65		0.4	Alluvial fan	
27	99.991 17	30.177 25		0.5–0.8	Alluvial fan	
28	99.966 61	30.187 86		2	Alluvial fan	
29	99.964 69	30.190 75	3.5–3.7		Gully	Loc. 4
30	99.963 81	30.191 25	4.1		Gully	Loc. 5
31	99.961 31	30.194 00		0.4–2.4	Alluvial fan	
32	99.940 36	30.205 00		0.9	Alluvial fan	
33	99.939 17	30.205 44		0.2–0.5	Alluvial fan	
34	99.923 61	30.218 61	3.6		Gully	Loc. 6
35	99.878 50	30.230 13	2.2		Gully	Loc. 7
36	99.870 75	30.232 17		0.2	Alluvial fan	

In the Damaoyaba Basin, the surface rupture zone begins near Jinchanggou in the southeast. Beyond Jinchanggou, it meanders along the piedmont on the northern rim of the Damaoyaba basin to the north of Heni Village for ~28 km. Near Jinchanggou, the rupture zone cuts through the I-level terrace on the south bank of the Wuliang River and forms landforms such as reverse scarps (~0.2–0.4 m high), sag ponds, swampy areas, and linear ridges. To the northwest, the rupture meanders along the piedmont on the northern edge of the Damaoyaba Basin and forms a series of landforms, including fault scarps, fault valleys, and piedmont slope break belts. The most recent scarps are ~0.2–0.3 m high. The ruptures are either new outcropping surfaces that follow turf tears and collapses at the tops of old scarps or series of gullies due to left-laterally offsets. The co-seismic horizontal displacements reach 2.2–4.1 m. The rupture zone extends to Heni Village. The strike gradually varies to NWW and nearly EW. The II-level terrace surface of the Wuliang River contains scarps ~0.2 m high that gradually disappear (Figs. 2a, 2b and Table 1).

We measured 36 co-seismic displacements of the surface rupture of the Litang fault along the Damaoyaba-Litang segment. Note that the co-seismic vertical displacements may include terrain effects that are caused by horizontal offsets and later-stage erosion. Hence, they can only be considered apparent displacements. Different researchers have interpreted different ages of the surface rupture. Tang and Han (1993) suggested that the surface rupture in the Litang Basin was a part of the $M7^1/_4$ earthquake in A.D. 1948. However, Xu et al. (2005) suggested that the surface rupture in the Litang Basin occurred in A.D. 1890, while the surface rupture on the northern edge of the Damaoyaba Basin was caused by another earthquake 119±2 a before present (A.D. 2005); i.e., in A.D. 1886±2. Based on our

detailed study of the two surface ruptures, we suggest that the 'freshness' of the two rupture zones, especially the free surface of the fault scarps, are consistent. They both show reverse strike-slip movements. The vertical displacement of the surface rupture along the northern edge of the Damaoyaba Basin is greater only because it is located at a bend in the fault. Therefore, the surface rupture zones in the Litang Basin and on the northern edge of the Damaoyaba Basin were all produced by the A.D. 1890 earthquake. Based on the 25-km-long surface rupture in the Litang Basin, the 28-km-long segment along the northern edge of the Damaoyaba Basin, and the 18-km-long middle segment, along which we did not find evidence of surface rupture, the total length of the surface rupture zone is 71 km. According to the empirical relationship between the earthquake magnitude (M_w), rupture length (L), and maximum co-seismic displacement (Dmax) (equation: M=6.81+0.78×lg D_{max}, Wells and Coppersmith, 1994), we estimate that the magnitude of the A.D. 1890 earthquake was M_w7.3±0.1.

2 EVIDENCE OF PALEOEARTHQUAKES

The Litang fault is located in the western Sichuan Plateau. The historical earthquake record is short; it only includes the M_w 7.3±0.1 earthquake swarm in A.D. 1890 and the M_s6.7 Batang earthquake swarm in A.D. 1989 (Xu et al., 2005; Zhou et al., 2005; EGDC, 1980). To clarify the recurrence behavior of large earthquakes on the Damaoyaba-Litang segment of the Litang fault, we excavated 5 trenches (Fig. 2). We used Trimble 5700 Differential Global Positioning System (GPS) to map the landforms in the study area. The ^{14}C samples were determined by the Accelerator Laboratory at Peking University and the Key Laboratory of Western China's Environmental Systems, Ministry of Education, Lanzhou University.

2.1 Litang Segment

We excavated 3 trenches along the Litang segment of the fault. Trenches Tc1 and Tc2 were located on the piedmont alluvial fan of Gari Mountain approximately 50 m from the trench excavated by Xu et al. (2005) (Figs. 5a, 5b). The alluvial fan formed on the piedmont due to a series of gullies from Gari Mountain that converge into the Litang Basin from SW to NE. The Litang fault cuts through the alluvial fan and forms reverse fault scarps (0.2–2 m high) and associated sag ponds. We excavated trenches Tc1 and Tc2 across the fault scarps. Trench Tc1 was 5 m long, 2.1 m wide, and 1.6–2.0 m deep. The stratigraphic sequence of the northwest wall of the trench is shown in Figs. 6, 9a.

Four paleoseismic events can be identified in Tc1. Event I occurred before B.C. 2755±65, but the precise date is unknown. Fault f1 is observed in layer ④ and overlain by layers ② and ③ sand veins from layer ③ were injected into the top of layer ④ on the southeast wall of the trench. We estimate that this was caused by the ground fissure that formed at the surface. Event II is represented by the displacements on faults f2 and possibly fault f3, which formed the sag-pond deposits of layer ② below the fault scarps. This earthquake occurred before B.C. 2755±65. Event III is represented by fault f2 and possibly fault f3. The f2 offset the sag-pond deposits of layer ② and extends to below layer ①. This earthquake occurred shortly after B.C. 1725±25. Event IV is represented by the displacement on f3, which extended to the ground surface, and it also formed the ground fissures of f4 and f5; this event was the A.D. 1890 earthquake.

Trench Tc2 was 6.4 m long, 2.7 m wide, and 1.6–2.2 m deep. The stratigraphic sequence of the northwest wall of the trench is shown in Figs. 7a, 9b, the southeast wall of the trench is shown in Figs. 7b, 10c.

Stratigraphic unit in SE wall and NW wall was almost the same in Tc2, only lack unit ⑧. The unit ⑧ was lenticle. The ^{14}C sampling age of these units in NW wall and SE wall was identical.

Five paleoseismic events can be identified in trench Tc2. Event I: the fault f1-4 offset layer ⑤ and was overlain by layer ④. The timing of the earthquake is unclear. Event II: the fault f5 offset layers ④ and ⑤ and was overlain by layer ③; the associated earthquake occurred before B.C. 2525±25. Event III caused additional displacements on fault f6 and formed the sag pond deposits of layer ②; the corresponding earthquake occurred between B.C. 1630±25 and B.C. 1340±25. Event IV caused additional displacements on fault f6 and formed the sag-pond deposits of layer ②, and fault f7 was displaced below the surface humus layer ①. This earthquake occurred between A.D. 1800±20 and B.C. 55±25 and was probably closer to B.C. 55±25. The sag-pond deposition stopped, which caused a deposition hiatus. Event V was the earthquake occurred in A.D. 1890.

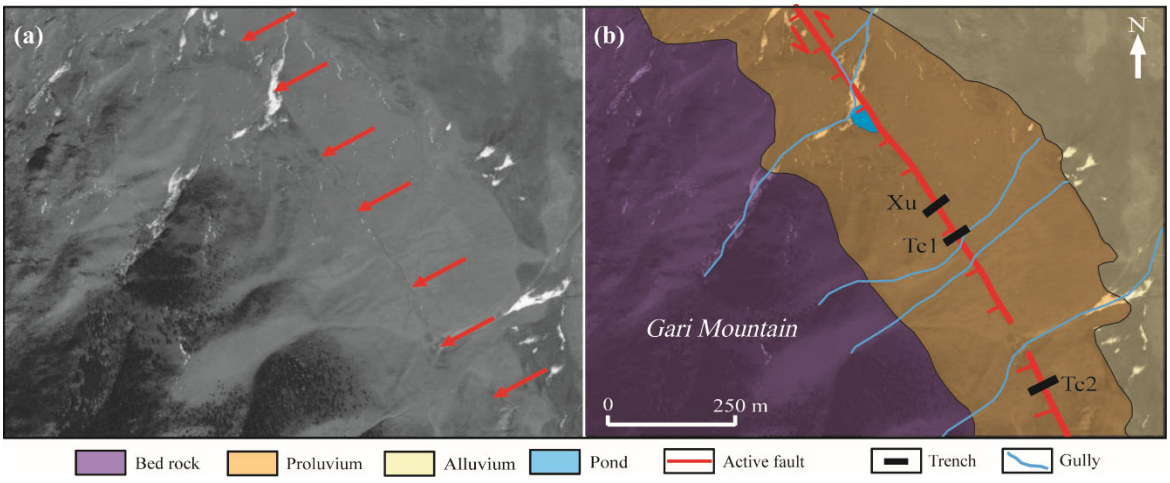

Figure 5. Trenching sites (a) aerial photo and (b) interpreted map, showing the tectonic landforms on the piedmont alluvial fan of Gari Mountain.

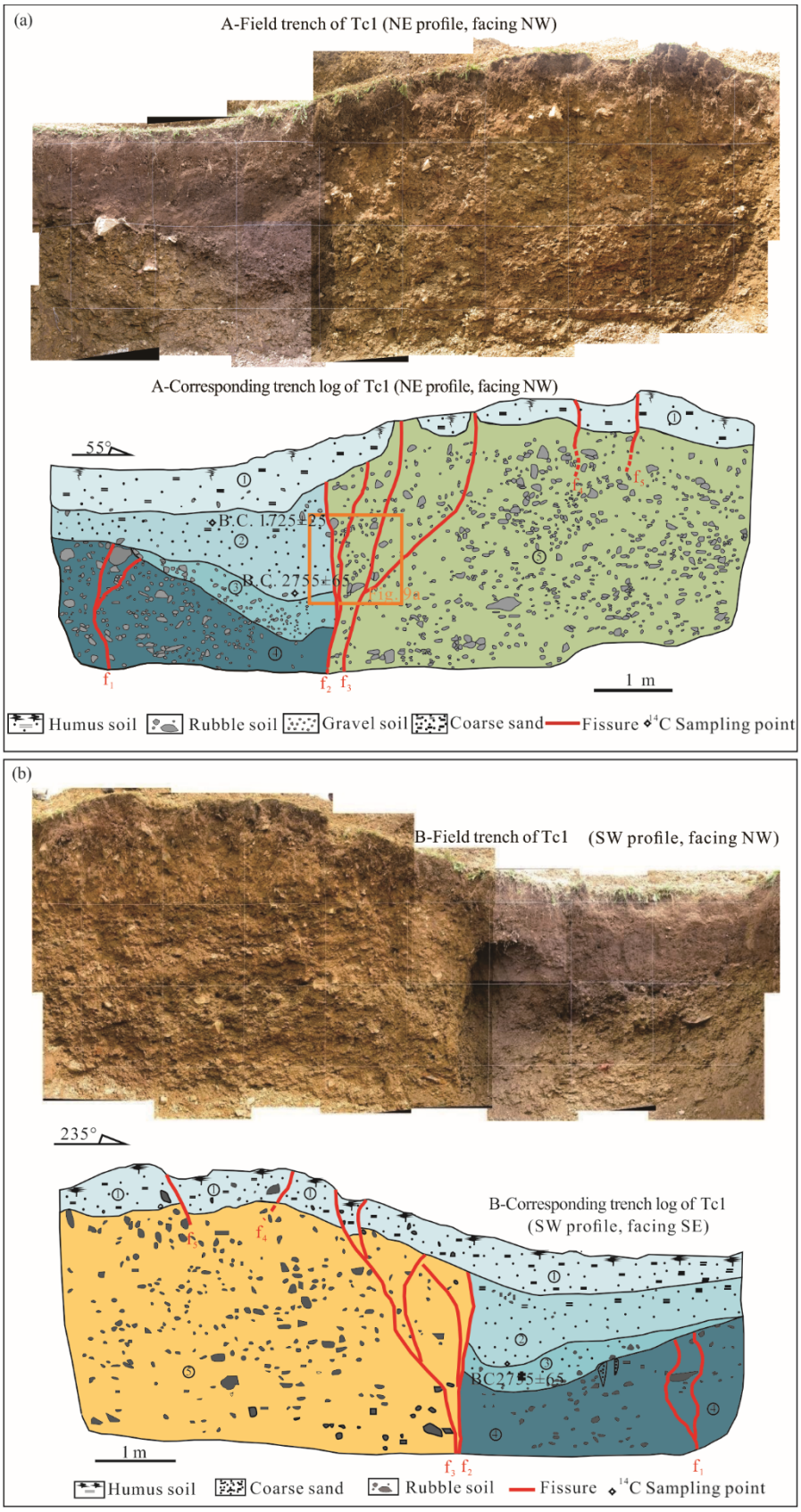

Figure 6. Photomosaic and interpreted map (northwest wall (a) and southeast wall (b)) of trench Tc1 on the piedmont alluvial fan of Gari Mountain. ① Dark-brown and gray-black humus with abundant plant roots and occasional gravels; ② sag-pond deposits composed of dark brown sand with abundant gravels (the ^{14}C age at the top of the deposit is B.C. 1725±25, and the ^{14}C age at the base of the deposit is B.C. 2755±65); ③ brown-yellow pluvial gravel and sand with especially high gravel content at the bottom; ④ isabelline pluvial gravel and sand (the gravels are unsorted and not rounded); ⑤ unsorted khaki pluvial gravel with minor bedding. A yellow rectangle indicates the location of enlarged photographs of Fig. 10a.

Trench Tc3 was located on the I-level terrace of the Wuliang River in the Litang Basin. It was 11 m long, 2.4 m wide, and 2.0–2.5 m deep. The stratigraphic sequence of the northwest wall of the trench is shown in Figs. 8, 9c.

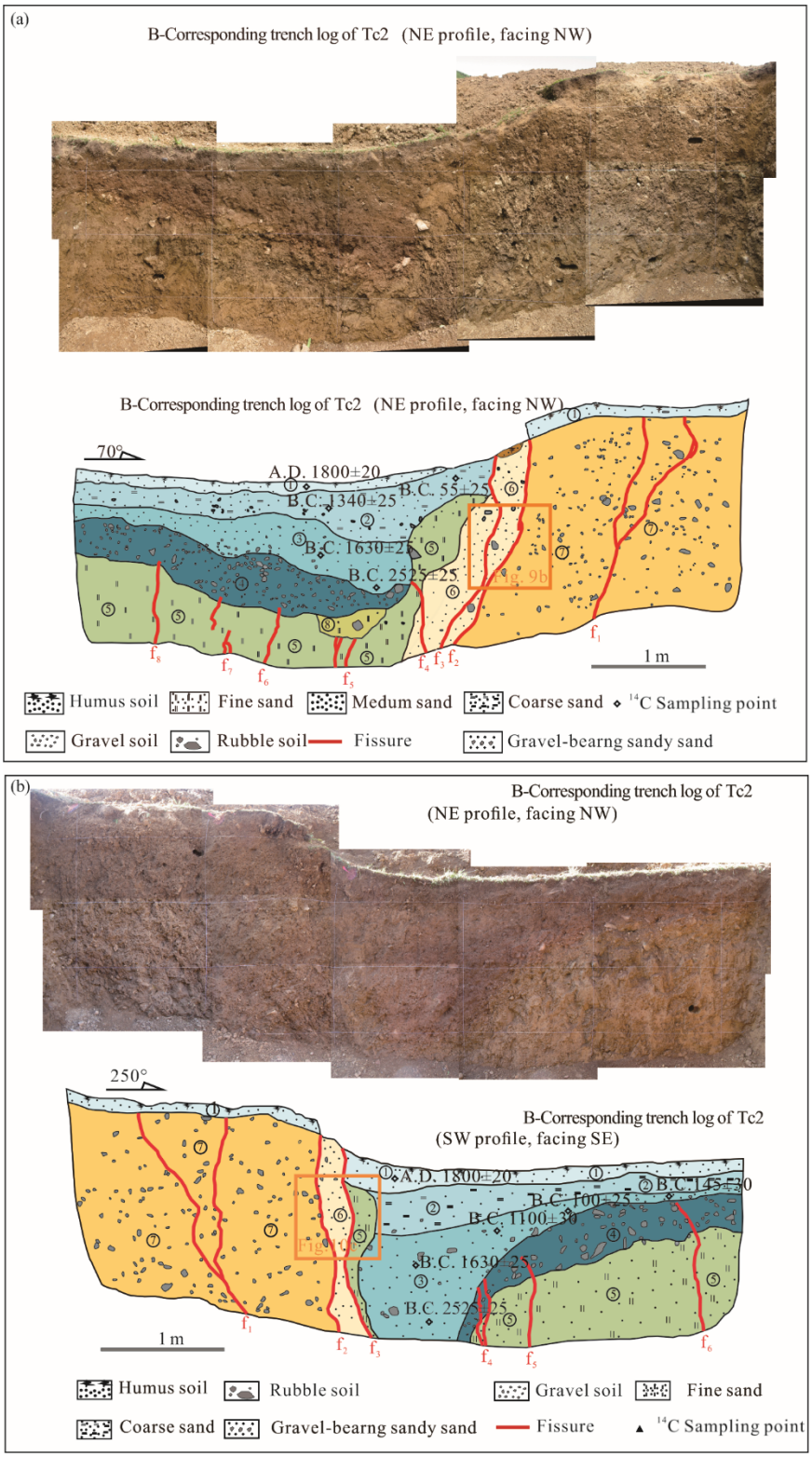

Figure 7. Photomosaic and interpreted map (northwest wall (a) and southeast wall (b)) of trench of trench Tc2 on the piedmont alluvial fan of Gari Mountain. ① Dark-brown and gray-black humus with abundant plant roots and occasional gravels; ② sag-pond deposits composed of dark brown pluvial sand with a few gravels (the ^{14}C age at the top of the deposit is B.C. 55±25, and the ^{14}C age of the middle is B.C. 1340±25); ③ tawny pluvial gravel and sand (the gravel content at the bottom is particularly high); ④ khaki pluvial gravel (the gravels are unsorted and not rounded); ⑤ khaki fine sand deposited in relatively quiet water; ⑥ khaki pluvial sand with gravels; ⑦ unsorted khaki pluvial gravel with minor bedding; ⑧ brown pluvial gravel and sand. A yellow rectangle indicates the location of enlarged photographs of Fig. 9b.

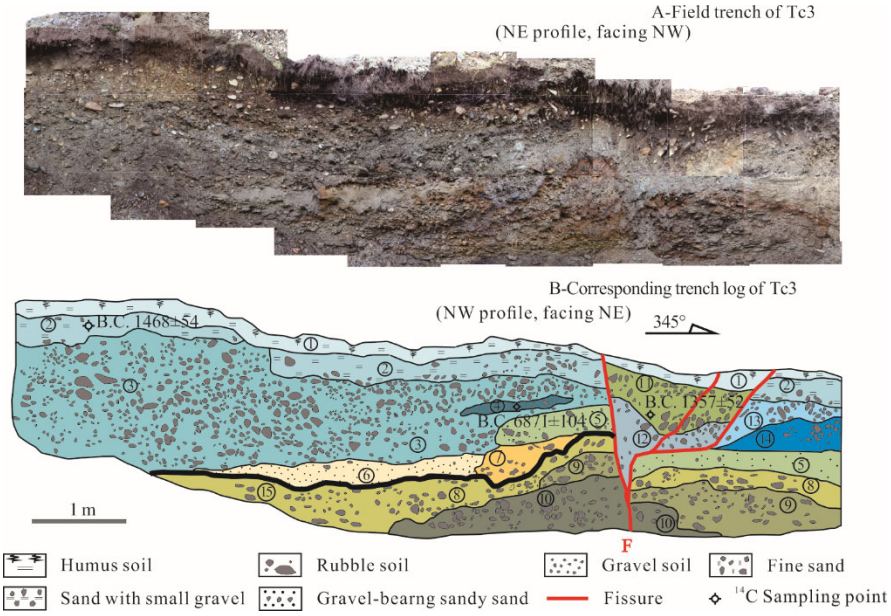

Figure 8. Photomosaic and interpreted map of the northwest wall of trench Tc3 on the I-level terrace of the Wuliang River in the Litang Basin. ① Dark-brown and gray-black humus with abundant plant roots and occasional gravels; ② dark brown and tawny fluvial sand with well-rounded small gravels (the ^{14}C age of the middle of the deposit is B.C. 1468±54); ③ khaki and livid well-rounded fluvial gravel; ④ lens of livid and gray-black fluvial fine sand; ⑤ livid well-rounded fluvial sand and gravel; ⑥ long lens of khaki and tawny coarse fluvial sand; ⑦ lens of livid fluvial sand and gravel; ⑧ brown fluvial gravel; ⑨ lens of brown fluvial sand and gravel; ⑩ khaki and tawny fluvial gravel (the gravel surfaces commonly have brown iron rust spots); ⑪ mixed deposit of dark brown sand and gravel, possibly a collapse deposit caused by an earthquake (the ^{14}C age at the bottom of the deposit is B.C. 1357±52); ⑫ colluvial wedge of livid sand and gravel deposited in front of scarp; ⑬ khaki fluvial gravel; ⑭ livid and gray-white fine fluvial gravel; ⑮ dark brown oxidation on an unconformity surface with an uneven thickness (maximum thickness is 5 cm). A yellow rectangle indicates the location of enlarged photographs of Fig. 9c.

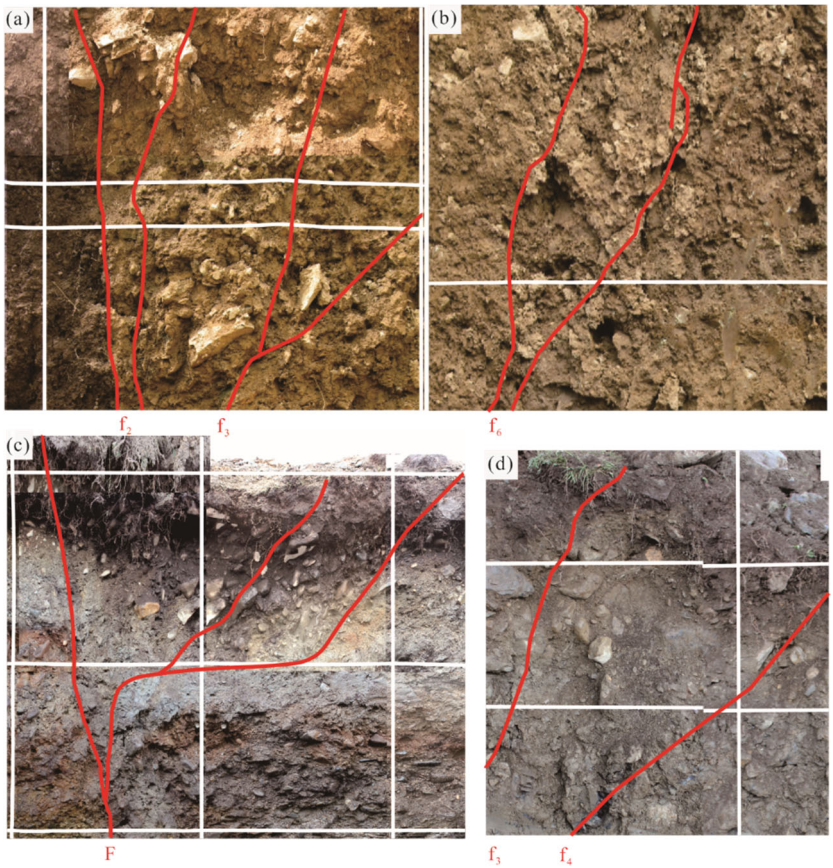

Figure 9. Enlarged photographs showing the details of the trench exposures; see the locations in Figs. 6, 7, 8, 11. (a) Fault planes f2 and f3 on the northwest wall of Tc1; (b) fault planes f2 and f3 on the northwest wall of Tc2; (c) master fault plane F on the northwest wall of Tc03; (d) fault planes f3 and f4 on the northwest wall of Tc4.

Three paleoseismic events can be identified in trench Tc3. Event I occurred on fault plane F and offset layers ⑩, ⑨, ⑧, and ⑤, formed fault scarps, and deposited the wedge of layer ⑫ in front of the scarps. The date of this earthquake is unclear. Event II also occurred on fault plane F and it offset layers ③ and ⑫, uplifted the fault scarps, and deposited the mixed deposit of layer ⑪ in front of the scarps. We interpret that this event also offset layer ②. This earthquake occurred between B.C. 1468±54 and B.C. 1357±52. Event III occurred on fault plane F and ruptured to the surface while forming several branching faults. Event III was the A.D. 1890 earthquake. Layer ⑤ is offset vertically by approximately 1 m across the trench, and the fault scarps on the surface are only 0.2–0.3 m high, which provides indirect evidence for multiple paleoseismic events.

Based on the results from trenches Tc1, Tc2, and Tc3 and the trench by Xu et al. (2005), the sequence of paleoseismic events on the Litang segment since B.C. 2525±25 (Fig. 13) is as follows.

Event I: Trench Tc2 indicated that this earthquake occurred between B.C. 1630±25 and B.C. 1340±25, while trench Tc3 indicated a date between B.C. 1468±25 and B.C. 1357±52. Trenches Tc2 and Tc3 may indicated the same earthquake, so the date of this event was between B.C. 1468±54 and B.C. 1340±25.

Event II: Trench Tc2 indicated that the earthquake occurred between A.D. 1800±20 and B.C. 55±25 and was probably closer to B.C. 55±25.

Event III: The Xu trench indicated that the earthquake occurred in A.D. 1115±90.

Event IV: Event IV represents the A.D. 1890 earthquake. The 4 trenches all show that the fault extended to the surface and formed surface rupture zones.

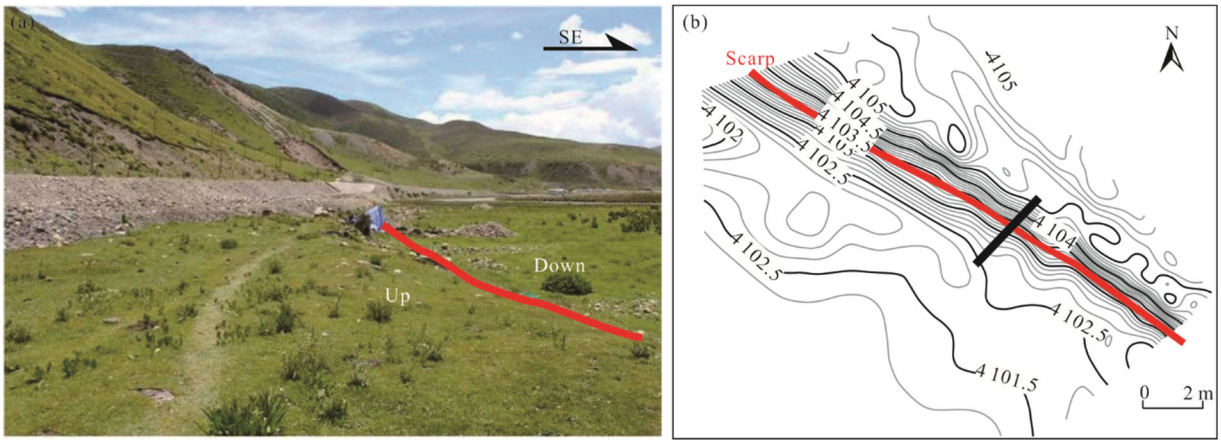

Figure 10. Landforms and map of trench Tc4 west of Jinchanggou. (a) View of the area around the trenching site, the red line indicates the fault trace; (b) topography around the trench site surveyed using differential GPS (RTK). The contour interval is 0.1 m.

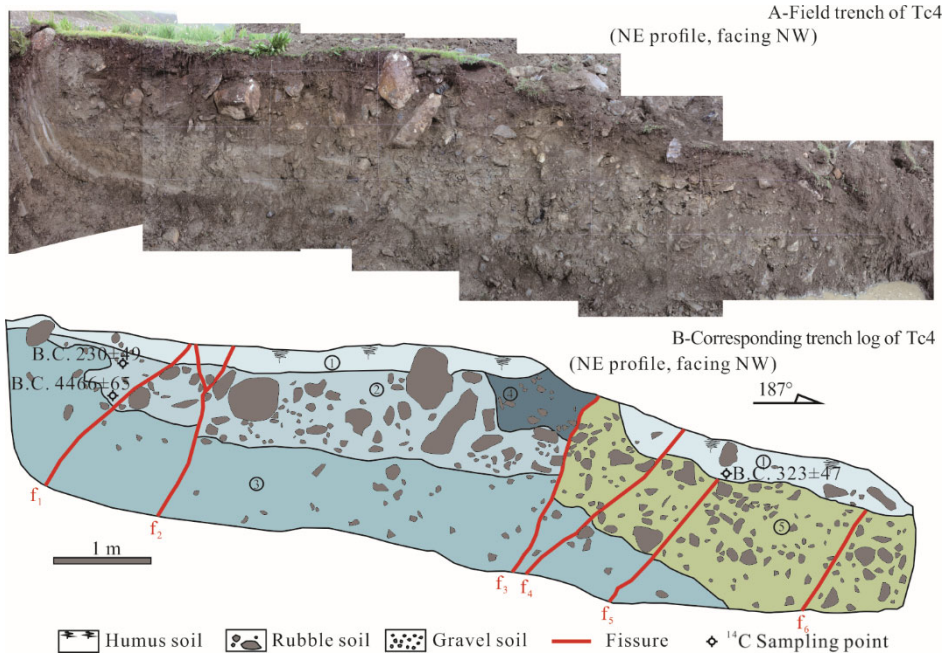

Figure 11. Photomosaic and interpreted map of the eastern wall of trench Tc4 to the west of Jinchanggou. ① Dark brown and gray black humus with abundant plant roots and occasional gravels (the ^{14}C age at the bottom is A.D. 323±47); ② gray black sand with gravels (the ^{14}C age at the top is B.C. 230±49, and the age at the bottom is B.C. 4466±65); ③ livid fluvial gravel and occasional large boulders with minor bedding in some locations; ④ dark brown fluvial sand and gravel; ⑤ gray and gray-white fluvial sand with abundant gravels. A yellow rectangle indicates the location of enlarged photographs of Fig. 9d.

2.2 Damaoyaba Segment

Two trenches along the Damaoyaba segment of the fault which cross the fault on the northern and southern edges of the Damaoyaba Basin were excavated. Trench Tc04 was located on the I-level terrace of the Wuliang River near Jinchanggou. The fault offset the I-level terrace and forms a scarp ~2 m high. Trench Tc4 (8 m long, 2.5 m wide, and 1.5–2.0 m deep) was excavated across the fault scarp (Fig. 10). The stratigraphic sequence revealed by the southeast wall is shown in Figs. 9d, 11.

Two paleoseismic events in trench Tc4 were identified. Event I: fault f1, f2, f5, f6 offset layers ⑤, ④, ③, and ② and was overlain by the surface humus layer ①. The earthquake occurred between B.C. 2 30±49 and A.D. 323±47. Event II: fault f3, f4 cut to the surface and formed earthquake rupture zones. Event II was the A.D. 1890 earthquake.

The fault on the southern edge of the basin forms a normal fault scarp ~0.5–1.0 m high on the pluvial fan. Trench Tc5 was excavated across the fault scarp; it is ~5 m long, 2 m wide, and 1.5 m deep. The stratigraphic sequence on the eastern wall of the trench is shown in Fig. 12.

Three paleoseismic events can be identified in trench Tc5. Event I displaced fault f4 and possibly fault f1 and formed the sag-pond deposits of layer ⑩. The earthquake occurred before A.D. 76±47. Event II displaced the fault below the surface humus layer ①. The earthquake occurred between A.D. 957±45 and the age of the base of the surface humus (i.e., after A.D. 957±45). Event III cut to the surface; it was the earthquake occurred in A.D. 1890.

Based on the data from trenches Tc4 and Tc5, we established the sequence of paleoseismic events on the Damaoyaba segment of the Litang fault (Fig. 13).

Event I: Trench Tc4 showed that this earthquake occurred between B.C. 230±49 and A.D. 323±47. Trench Tc5 reveals an earthquake that occurred before A.D. 76±47, which we interpreted to have occurred between B.C. 230±49 and A.D. 76±47.

Event II: Trench Tc5 showed that this earthquake occurred after A.D. 957±45.

Event III: This event is the earthquake in A.D. 1890.

A comparison of the sequence of paleoseismic events in the Damaoyaba segment and Litang segment of the Litang fault (box in Fig. 13) shows that the dates of the three most recent paleoearthquakes are consistent. Thus, the sequence of paleoseismic events of the Litang fault can be determined as

Event I: occurred between B.C. 1340±25 and B.C. 1468±54.

Event II: occurred between B.C. 55±25 and A.D. 76±47.

Event III: occurred in A.D. 1115±90. Because the ^{14}C sample from the Damaoyaba segment was collected from the middle of the sag-pond deposits, while the ^{14}C sample from the Litang segment was collected from the top of the faulted strata, the latter is more representative of the actual date of the earthquake.

Event IV: occurred in A.D. 1890.

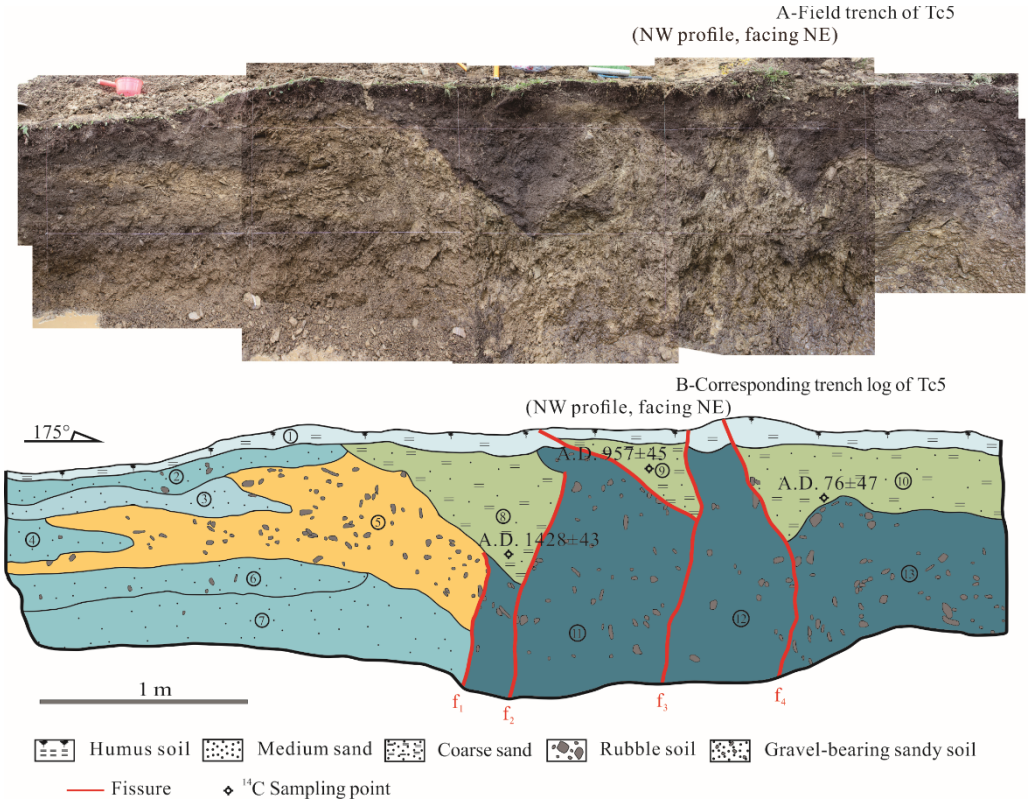

Figure 12. Photomosaic and interpreted map of the eastern wall of trench Tc5 on the southern edge of the Damaoyaba Basin. ① Gray-black humus with abundant plant roots and occasional gravels; ② unsorted dark brown sand and gravel; ③ brown pluvial sand with abundant gravels; ④ brown pluvial sand and gravel; ⑤ unsorted khaki pluvial gravel (the gravels were disorderly deposited); ⑥ gray-black pluvial sand and gravel; ⑦ tawny coarse pluvial sand with a few gravels and minor bedding; ⑧ triangular wedge of black sand sag-pond deposits (the ^{14}C age at the bottom is A.D. 1428±43); ⑨ triangular wedge of black sand sag-pond deposits (the ^{14}C age in the middle and upper part is A.D. 957±45); ⑩ sag-p5nd deposits composed of black sand with gravels (the ^{14}C age at the base is A.D. 76±47). Layers ⑪ was layer of unsorted khaki pluvial gravels that are disordered and fluvial in origin.

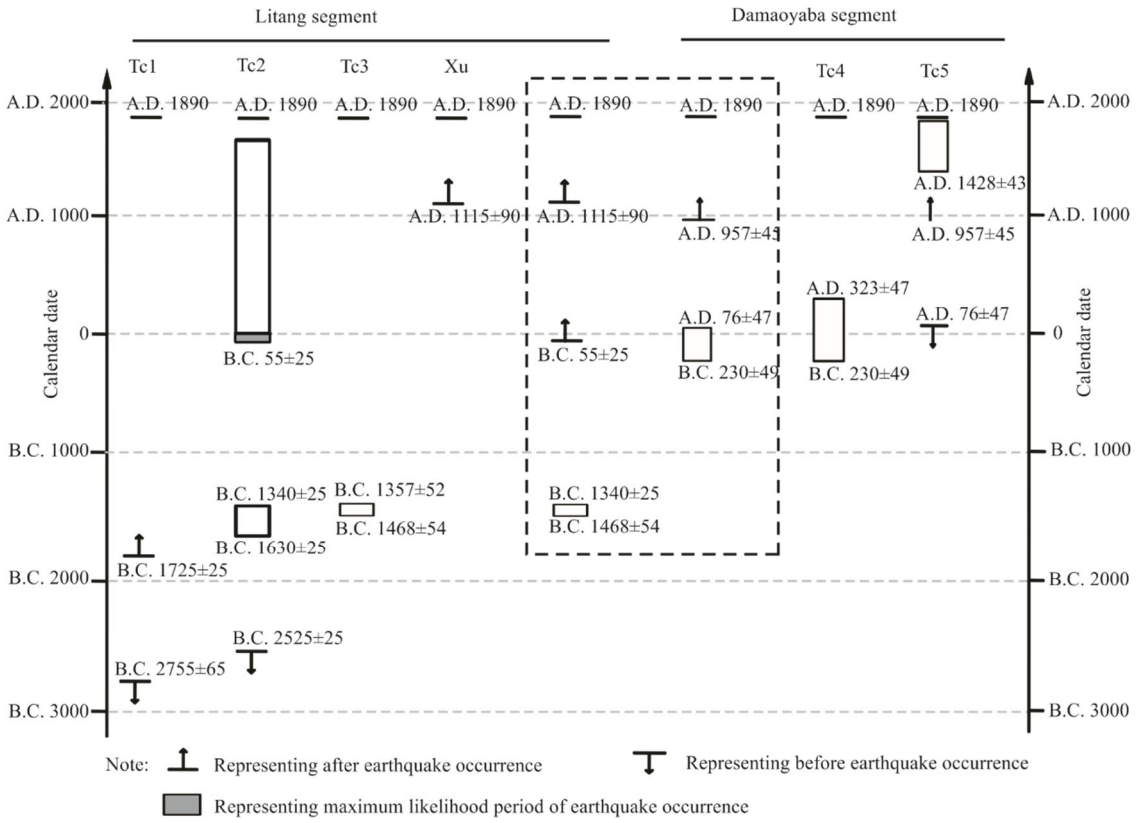

Figure 13. The sequence of paleoseismic events along Litang-Damaoyaba segment of the Litang fault.

Therefore, the recurrence intervals between the 4 paleoearthquakes on the Damaoyaba and Litang segments of the Litang fault are 1 415±80, 1 104±104, and 775±90 a. The recurrence behavior is consistent with a quasi-periodic recurrence pattern (Wen, 1995; Shimazaki and Nakata, 1980). The average recurrence interval is 1 098±112 a.

3 DISCUSSION

The spatial distributions of the historical co-seismic surface ruptures and the sequence of paleoseismic events indicate that the Damaoyaba and Litang segments of the Litang fault represent a unified earthquake rupture unit. Thus, a question to address is why the surface rupture zone of the A.D. 1890 earthquake has a discontinuity or gap of approximately 18 km between the Damaoyaba segment and the Litang segment. First, the segment in which we did not identify a surface rupture is located between Jinchanggou and west of Cunge Village. This segment is where the mountain and valley areas are deeply cut by the Wuliang River. The original surface rupture may not have been preserved because of erosion. An example of a similar earthquake is the M_w7.6 Luhuo earthquake in 1973. The Luhuo earthquake formed a surface rupture approximately 90 km long that is now preserved in only a few place, such as Yousi. Most parts of the rupture can no longer be identified. In addition, the A.D. 1890 earthquake may have two large-strain or high-stress release zones at Damaoyaba and Litang. The segment between Jinchanggou and west of Cunge Village may not have ruptured at the surface because of the small strain release and active faults had absorb the displacement along the rim of fault (Liu et al., 2020). This can also be verified by the 18-km-long gap between the eastern and western surface ruptures of the M_w7.1 Yushu earthquake in 2010 (Chen et al., 2010). Based on the horizontal slip rate of the fault on the northern rim of the Damaoyaba Basin (4.1±0.9 mm/yr) and the co-seismic displacement of 4.1 m in A.D. 1890 (Xu et al., 2005), the earthquake recurrence equation T=D/V (Wallace, 1970) gives a recurrence interval of large earthquakes of 1 050±230 a. Based on the horizontal fault slip in the Litang Basin of 3.8–4.4 mm/yr (Zhou et al., 2005) and the co-seismic displacement of 4 m in A.D. 1890, we estimate that the recurrence interval of large earthquakes is 981±72 a. These estimates are generally consistent with the recurrence intervals of the sequence of paleoseismic events that was identified in the trenches. Considering the Damaoyaba and Litang segments of the Litang fault as unified seismic rupture units, the recurrence intervals are 1 415±80, 1 104±104, and 775±90 a between the 4 paleoearthquakes. The recurrence behavior is consistent with a quasi-periodic recurrence pattern (Wen, 1995; Shimazaki Nakata, 1980). The average recurrence interval is 1 098±112 a.

4 CONCLUSIONS

(1) The traces of the latest surface activity along the Litang fault in west of Litang consist of three different segments: the Cuopuhu segment, Damaoyaba segment, and Litang segment. The fact that the surface rupture of the A.D. 1890 earthquake was only located along the Damaoyaba and Litang segments indicates that the Haizi Mountain uplift formed an obstruction that prevented earthquake propagation, while the large-angle bending and branching of the fault near Jinchanggou is not a boundary of the earthquake rupture. The M_w7.3 earthquake demonstrated that the Litang fault plays an important role in the

crustal deformation within the Sichuan-Yunnan active block. The Litang earthquake releases the accumulated stress of the India-Eurasia plate collision.

(2) The Damaoyaba and Litang segments of the Litang fault form a unified earthquake rupture unit that has quasi-periodic recurrence behavior for large earthquakes. However, due to the limited objectives and funding of this study, we did not conduct a combined trench study, and the co-seismic displacement of each paleoseismic event has not yet been precisely determined. Thus, the data are insufficient to support the conclusions presented above. In particular, although the Cuopuhu segment does not show recent co-seismic surface rupture, the clear fault landforms indicate significant earthquake displacements. The Litang fault has a relatively high risk of the recurrence of large earthquakes in the future and is worth further study.

ACKNOWLEDGMENTS

This research was supported by the "China Seismic Active Fault Exploration, Central-South Segment Project of the North-South Seismic Belt" of the China Earthquake Administration and the National Science Foundation of China (No. 41372114). Our thanks go to Prof. Xiwei Xu, Qinjian Tian and Mengtan Gao for their guidance and assistance in the field. We are grateful to the understanding and cooperation by the Tibetans in the study region. The final publication is available at Springer via https://doi.org/10.1007/s12583-021-1425-z.

REFERENCES CITED

Chen, L. C., Wang, H., Ran, Y. K., et al., 2010. The M_s7.1 Yushu Earthquake Surface Rupture and Large Historical Earthquakes on the Garzê-Yushu Fault. *Chinese Science Bulletin*, 55(31): 3504–3509. https://doi.org/10.1007/s11434-010-4079-2

Chevalier, M. L., Leloup, P. H., Replumaz, A., et al., 2016. Tectonic-Geomorphology of the Litang Fault System, SE Tibetan Plateau, and Implication for Regional Seismic Hazard. *Tectonophysics*, 682: 278–292. https://doi.org/10.1016/j.tecto.2016.05.039

EGDC (The Editorial Group of the Data Compilation of Earthquakes in Sichuan), 1980. The Data Compilation of Earthquakes in Sichuan. Sichuan People's Press, Chengdu (in Chinese)

He, Z. T., Ma, B. Q., Long, J. Y., et al., 2018. New Progress in Paleoearthquake Studies of the East Sertengshan Piedmont Fault, Inner Mongolia, China. *Journal of Earth Science*, 29(2): 441–451. https://doi.org/10.1007/s12583-017-0937-z

Liu, X. W., Yuan, D. Y., Su, Q., et al., 2020. Late Quaternary Tectonic Activity and Slip Rates of Active Faults in the Western Hexi Corridor, NW China. *Journal of Earth Science*, 31(5): 968–977. https://doi.org/10.1007/s12583-020-1287-9

Molnar, P., Tapponnier, P., 1975. Cenozoic Tectonics of Asia: Effects of a Continental Collision: Features of Recent Continental Tectonics in Asia can be Interpreted as Results of the India-Eurasia Collision. *Science*, 189(4201): 419–426. https://doi.org/10.1126/science.189.4201.419

Shimazaki, K., Nakata, T., 1980. Time-Predictable Recurrence Model for Large Earthquakes. *Geophysical Research Letters*, 7(4): 279–282. https://doi.org/10.1029/gl007i004p00279

Tang, R. C., Han, W. B., 1993. Active Faults and Earthquakes in Sichuan. Seismological Press, Beijing (in Chinese)

Tapponnier, P., 2001. Oblique Stepwise Rise and Growth of the Tibet Plateau. *Science*, 294(5547): 1671–1677. https://doi.org/10.1126/science.105978

Wallace, R. E., 1970. Earthquake Recurrence Intervals on the San Andreas Fault. *Geological Society of America Bulletin*, 81(10): 2875. https://doi.org/10.1130/0016-7606(1970)81[2875: eriots]2.0.co;2

Wells, D. L., Coppersmith, K. J., 1994. New Empirical Relationships among Magnitude, Rupture Length, Rupture Width, Rupture Area, and Surface Displacement. *Bull. Seismol. Soc. Am*., 84(4): 974–1002

Wen, X. Z., 1995. Quantitative Estimates of Seismic Potential on Active Faults. Seismological Press, Beijing (in Chinese)

Xu, X. W., Wen, X. Z., Yu, G. H., et al., 2005. Average Slip Rate, Earthquake Rupturing Segmentation and Recurrence Behavior on the Litang Fault Zone, Western Sichuan Province, China. *Science in China Series D*: *Earth Sciences*, 48(8): 1183–1196. https://doi.org/10.1360/04yd0072

Xu, X. W., Wen, X. Z., Zheng, R. Z., et al., 2003. Pattern of Latest Tectonic Motion and Its Dynamics for Active Blocks in Sichuan-Yunnan Region, China. *Science in China Series D*: *Earth Sciences*, 46(2): 210–226. https://doi.org/10.1360/03dz0017

Yan, B., Toda, S., Lin, A. M., 2018. Coulomb Stress Evolution History as Implication on the Pattern of Strong Earthquakes along the Xianshuihe-Xiaojiang Fault System, China. *Journal of Earth Science*, 29(2): 427–440. https://doi.org/10.1007/s12583-018-0840-2

Zhang, P. Z., Deng, Q. D., Zhang, Z. Q., et al., 2013. Active Faults, Earthquake Hazards and Associated Geodynamic Processes in Continental China. *Science China Earth Science*, 43: 1607–1620 (in Chinese with English Abstract)

Zhou, R. J., Chen, G. X., Li, Y., et al., 2005. Research on Active Faults in Litang-Batang Region, Western Sichuan Province, and the Seismogenic Structures of the 1989 Batang *M*6.7 Earthquake Swarm. *Seismol. Geol*., 27(1): 31–43 (in Chinese with English Abstract)

Zhou, R. J., Ye, Y. Q., Li, Y., et al., 2007. Late-Quaternary Activity of the Shawan Segment of the Litang Faults. *Quaternary Sciences*, 27(1): 45–53 (in Chinese with English Abstract)